THE ASTROPHYSICAL JOURNAL, 555:477–482, 2001 July 1
© 2001. The American Astronomical Society. All rights reserved. Printed in U.S.A.

COMPLETE AND SIMULTANEOUS SPECTRAL OBSERVATIONS OF THE BLACK HOLE X-RAY NOVA XTE J1118+480

J. E. MCCLINTOCK,[1] C. A. HASWELL,[2] M. R. GARCIA,[1] J. J. DRAKE,[1] R. I. HYNES,[3] H. L. MARSHALL,[4] M. P. MUNO,[4] S. CHATY,[2] P. M. GARNAVICH,[5] P. J. GROOT,[1] W. H. G. LEWIN,[4] C. W. MAUCHE,[6] J. M. MILLER,[4] G. G. POOLEY,[7] C. R. SHRADER,[8] AND S. D. VRTILEK[1]

Received 2000 October 28; accepted 2001 March 5

ABSTRACT

The X-ray nova XTE J1118+480 suffers minimal extinction ($b = 62°$) and therefore represents an outstanding opportunity for multiwavelength studies. Hynes et al. conducted the first such study, which was centered on 2000 April 8 using UKIRT, *EUVE*, *HST*, and *RXTE*. On 2000 April 18, the *Chandra X-Ray Observatory* obtained data coincident with a second set of observations using all of these same observatories. A 30 ks grating observation using *Chandra* yielded a spectrum with high resolution and sensitivity covering the range 0.24–7 keV. Our near-simultaneous observations cover $\approx 80\%$ of the electromagnetic spectrum from the infrared to hard X-rays. The UV/X-ray spectrum of XTE J1118+480 consists of two principal components. The first of these is an ≈ 24 eV thermal component that is caused by an accretion disk with a large inner disk radius: $\gtrsim 35 R_{\rm Schw}$. The second is a quasi power-law component that was recorded with complete spectral coverage from 0.4 to 160 keV. A model for this two-component spectrum is presented in a companion paper by Esin et al.

Subject headings: accretion, accretion disks — binaries: close — stars: individual (XTE J1118+480) — ultraviolet: stars — X-rays: stars

1. INTRODUCTION

X-ray novae (a.k.a. soft X-ray transients) are a type of X-ray binary that typically remains quiescent for decades before brightening by as much as 10^7 in X-rays in a week. In outburst, the 2–10 keV X-ray spectrum of most X-ray novae is dominated by thermal emission from the inner accretion disk. However, we now know of five X-ray novae that have failed to show this soft thermal component during outburst (Brocksopp et al. 2001). One of these five is XTE J1118+480. This source is further distinguished by its strikingly low X-ray–to–optical flux ratio (Hynes et al. 2000).

XTE J1118+480 was discovered on 2000 March 29 (Remillard et al. 2000). During the month of March, the *Rossi X-Ray Timing Explorer* (*RXTE*) All-Sky Monitor data show that the X-ray intensity of the source increased steadily to ≈ 35 mcrab (2–12 keV). Thereafter, the intensity remained near that level for about three months before declining abruptly. The optical counterpart brightened from quiescence by about 6 mag to $V \approx 13$ (Uemura et al. 2000). Optical observations in outburst and quiescence confirm that the orbital period is 4.08 hr (Patterson 2000; Uemura et al. 2000; McClintock et al. 2001; Wagner et al. 2001). A radio counterpart has also been observed (Pooley & Waldram 2000). The most uncommon property of XTE J1118+480 is its exceptionally high galactic latitude, $b = +62°$ and its correspondingly low reddening: $E(B-V) \approx 0.013$ mag ($N_{\rm H} \approx 7.5 \times 10^{19}$ cm^{-2}; Hynes et al. 2000). XTE J1118+480 is the least reddened of all known X-ray binaries.

Recently, dynamical measurements by two groups have established that XTE J1118+480 has a very large mass function, which sets a hard lower limit of $6\,M_\odot$ on the mass of the compact X-ray source (McClintock et al. 2001; Wagner et al. 2001). Since this greatly exceeds the maximum allowed stable mass of a neutron star in general relativity (Rhoades & Ruffini 1974), we refer to the compact primary as a black hole.

The first epoch of an intensive multiepoch, multiwavelength observing campaign was reported by Hynes et al. (2000). Here we report on the second-epoch observations, centered on 2000 April 18, which are unique in including a 0.24–7 keV grating spectrum obtained using the *Chandra X-Ray Observatory* (*Chandra*). This spectrum is very important and forces modification of the conclusions reached by Hynes et al. (2000). Our near-simultaneous observations cover $\approx 80\%$ of the electromagnetic spectrum from the infrared to hard X-rays; these multiwavelength data are modeled in a companion paper by Esin et al. (2001).

2. NEAR-SIMULTANEOUS OBSERVATIONS

A journal of the near-simultaneous observations made on or near April 18 is given in Table 1. The April 18 *Extreme Ultraviolet Explorere* (*EUVE*) data are discussed extensively by Hynes et al. (2000), but they were not used in their spectral energy distribution (SED). The only data in common between the SED presented by Hynes et al. and the SED presented here is the April 18 UKIRT data. In the following, we briefly discuss each data set in turn.

[1] Harvard-Smithsonian Center for Astrophysics, 60 Garden Street, Cambridge, MA 02138; jem@cfa.harvard.edu, mgarcia@cfa.harvard.edu, jdrake@cfa.harvard.edu, pgroot@cfa.harvard.edu, svrtilek@cfa.harvard.edu.

[2] Department of Physics and Astronomy, The Open University, Walton Hall, Milton Keynes MK7 6AA, UK; c.a.haswell@open.ac.uk, s.chaty@open.ac.uk.

[3] Department of Physics and Astronomy, University of Southampton, Southampton SO17 1BJ, UK; rih@astro.soton.ac.uk.

[4] Center for Space Research, MIT, Cambridge, MA 02139; hermanm@space.mit.edu, muno@space.mit.edu, lewin@space.mit.edu, jmm@space.mit.edu.

[5] Physics Department, University of Notre Dame, Notre Dame, IN 46556; pgarnavi@nd.edu.

[6] Lawrence Livermore National Laboratory, L-43, 7000 East Avenue, Livermore, CA 94550; mauche@cygnus.llnl.gov.

[7] Mullard Radio Astronomy Observatory, Cavendish Laboratory, Madingley Road, Cambridge CB3 0HE, UK; ggp1@cam.ac.uk.

[8] Laboratory for High-Energy Astrophysics, NASA Goddard Space Flight Center, Greenbelt, MD 20771; shrader@grossc.gsfc.nasa.gov.

TABLE 1

OBSERVATIONS ON OR NEAR 2000 APRIL 18 UT

Observatory	Instrument	Bandpass	log (ν)	Observation Interval (UT)	Net Observing Time (ks)
RXTE	HEXTE	15–200 keV	18.56–19.68	18 Apr 19:28–18 Apr 23:00	1.1
	PCA	2.5–25 keV	17.78–18.78	18 Apr 19:28–18 Apr 23:00	2.8
Chandra	LETG/ACIS-S	0.24–7 keV	16.76–18.23	18 Apr 18:16–19 Apr 02:16	27.2
EUVE	SW	0.10–0.17 keV	16.38–16.61	16 Apr 21:34–19 Apr 14:28	81.1
HST	STIS	1155–10250 Å	14.47–15.41	18 Apr 13:40–18 Apr 17:44	6.2
UKIRT.....	IRCAM/TUFTI	1–5 μ	13.78–14.48	18 Apr 12:00	0.01–0.06
Ryle Telescope.....	15.2 GHz receiver	2.0 cm	10.18	18 Apr 17:11–18 Apr 18:36	5.1

RXTE spectra were produced using 128 channel Proportional Counter Array (PCA) data collected with PCUs 0, 2, and 3, and 64 channel data collected with the HEXTE (High-Energy X-Ray Timing Experiment) clusters A and B. Following the suggestions of Jahoda (2000), we have selected only the top layers of each PCU and have combined the data for all three PCUs. A response matrix was generated using version 2.43 of "pcarsp," and a background estimate was generated using the 2000 January 31 blank-sky model for gain epoch 4 combined with version 2.1e of "pcabackest." A 1% systematic error was added to the statistical error estimate and each model was fit between 2.5 and 25 keV. This systematic error was required because the statistical uncertainty for the PCA is significantly less than the uncertainty in the PCA response matrix, which is estimated to be about 1% (Jahoda 2000). For the HEXTE we used the standard response matrices and modeled the data between 15 and 200 keV, allowing for a constant normalization between the PCA data and the data from the two HEXTE clusters. No systematic errors were added to these data. The background was estimated using the script "hxtback" from FTOOLS version 5. The combined PCA and HEXTE data are compatible with a power-law model for the emission. The best-fit photon index was $\Gamma = 1.782 \pm 0.005$ with a 2–200 keV flux of 4.2×10^{-9} ergs cm^{-2} s^{-1} and a χ^2 of 164 for 139 degrees of freedom (dof). The photon index is consistent with the value measured 10 days earlier: $\Gamma = 1.8 \pm 0.1$ (Hynes et al. 2000). A Gaussian feature at 6.4 keV was evident in the residuals to the fit ($\chi^2 = 152$ for 136 dof) with an equivalent width (EW) of 40 eV. This feature is very probably not caused by the source for two reasons. First, its strength is consistent with a feature seen in fits to the spectrum of the Crab Nebula, where no Fe-K line is expected; thus it is probably a systematic feature in the response matrices that we used (Jahoda 2000). Second, the feature does not appear in the *Chandra* grating data described directly below. For an assumed narrow 6.4 keV line, $\Delta E/E = 0.04$, the *Chandra* data imply a 3 σ upper limit of EW < 24 eV, which strongly rules against the *RXTE* candidate Fe line. For a broader assumed line width, $\Delta E/E = 0.10$, the *Chandra* 3 σ upper limit is EW < 38 eV, which marginally rules against the *RXTE* spectral feature. On the other hand, a very broad line, with a width comparable to the energy resolution of the PCA detector ($\Delta E/E \approx 0.2$) and an EW of 40 eV would have escaped detection by *Chandra*.

Chandra observations were performed using the Low Energy Transmission Grating (LETG) and the ACIS-S detector, which yielded a spectrum from 0.24 to 7 keV (1.8–52 Å) with a resolution of about 0.04 Å. The "Level 1" data were reduced using custom IDL procedures in several steps: (1) sky coordinates were transformed to grating coordinates by correcting for spacecraft roll; (2) the location of zeroth order was determined by fitting a pair of one-dimensional Gaussian profiles; (3) pulse height was converted to energy ($E_{\rm PH}$) using preflight gains and then corrected (node by node) to match the energies inferred from the dispersion of the LETG; and (4) events were selected using $r_l < E_{\rm PH}/E_{\rm LETG} < r_h$, where r_l, r_h was [0.70, 1.15] for +1 events, [0.80, 1.20] for −1 events with $\lambda < 30$ Å, and [0.65, 1.25] for −1 events with $\lambda > 30$ Å. These selections net greater than 99% of the observed counts. All events within 2.″5 of the dispersion line were included, except for the events near detector gaps, which were ignored. Any aperture size between 1.″5 and 3″ would have yielded the same results. No background was subtracted because the background rates were negligible compared to the source rates (<1%), except near the C-K edge, where the background rate was up to 5% of the source rate. The events were binned and the effective areas were integrated over the bins. After correcting for the fraction of counts dispersed by the LETG fine support structure, we estimate that the fluxes are accurate to ∼5% in the 2–5 keV range. XTE J1118+480 was the brightest source observed with this grating and detector combination, so these data are being used extensively to verify and update the instrumental area, which could still have systematic errors of order 10%–20% in the 0.2–1.0 keV band (Marshall 2001).[9] The largest uncertainties are in the 0.3–0.5 keV band. The spectrum was searched at high resolution (0.01 Å) for lines and edges with assumed widths comparable to the instrumental resolution. None was found apart from two weak, unidentified lines, 13.24 Å (0.936 keV) and 9.36 Å (1.325 keV), which were detected at significance levels of 5.6 and 4.6 σ, respectively; the latter feature was detected only in the third-order spectrum. The probability of finding a feature in one bin at ≥ 4.6 σ among the 2500 bins searched is only 0.5%. The complete high-resolution spectrum is shown in Figure 1. Given the near absence of spectral features, the data were binned heavily on a logarithmic grid ($\Delta E/E = 0.02$) to provide an accurate measure of the continuum. On timescales $\gtrsim 1$ ks, the total X-ray intensity was constant to ∼3% during the 27 ks observation. For the energy range 2–7 keV, the power-law photon index was $\Gamma = 1.77 \pm 0.04$, which is consistent with the *RXTE* values quoted above.

EUVE observations were performed 3 arcmin off-axis to extend the wavelength coverage of the *EUVE* short-wavelength spectrometer (SW) shortward of its normal cutoff (Marshall et al. 1996). Data from the SW spectro-

[9] Marshall, H. L. 2001, unpublished, (LETG/ACIS-S calibration web site: http://space.mit.edu/CXC/calib/letg_acis/ck_cal.html)

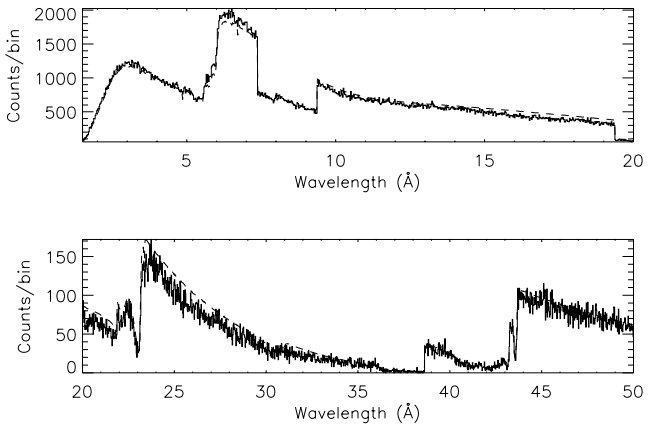

FIG. 1.—First-order ACIS/LETG count spectrum binned at 0.025 Å as obtained in a 27 ks observation with *Chandra*. The dashed line corresponds to a power-law model spectrum folded through the instrument response with $\Gamma = 1.78$ (§ 3) and $N_H = 1.3 \times 10^{20}$ cm^{-2}. Apart from a weak, unidentified feature centered at 13.24 Å (§ 2), this first-order spectrum is devoid of lines.

meter were binned in 2 Å intervals and corrected for interstellar (IS) absorption using the compilation of H and He photoionization cross sections of Rumph, Bowyer, & Vennes (1994), with a mixture of neutral hydrogen to neutral and ionized helium in the ratio 1:0.1:0.01. Fortunately, the shape of the extinction curve is largely independent of these details of the gas mix. Flux calibration was achieved using the filter-corrected exposure time and the off-axis effective area curve of H. Marshall et al. (2001, in preparation). An independent analysis of these data is discussed by Hynes et al. (2000); there are no significant differences between their extracted spectrum and the one presented herein.

Hubble Space Telescope (*HST*) observations were made using the Space Telescope Imaging Spectrograph (STIS) and the E140M, E230M, G430L, and G750L gratings. An average calibrated spectrum for April 18 was constructed from standard *HST* pipeline data products. The spectrum exhibits emission lines of Hα (weak), He II (1640, 4686 Å), Si IV (1394, 1403 Å) and N V (1239, 1243 Å), as well as Lyα, higher order Balmer lines, and the Balmer jump in absorption. To identify the continuum spectrum more clearly, and remove near-infrared (NIR) fringing, the spectra were rebinned with the regions dominated by Lyα and N V masked out.

The 3.8 m United Kingdom Infrared Telescope (UKIRT) was used to make NIR photometric observations at *JHKLM* with IRCAM/TUFTI. The measured magnitudes and comments on the data analysis can be found in Hynes et al. (2000).

The Ryle Telescope was used to monitor the flux density at 15.2 GHz using techniques similar to those described in Pooley & Fender (1997). The phase calibrator used was J1110+440, and the flux-density scale was established by observations of 3C 48 and 3C 286.

3. SUPPORTING OBSERVATIONS

The intensity of XTE J1118+480 was relatively constant during the 81 ks *EUVE* observation (Hynes et al. 2000) and during the 27 ks *Chandra* observation (§ 2). In addition, the source was very stable on timescales $\gtrsim$ hours at all wavelengths for weeks before and after our April 18 observing campaign. To illustrate this constancy, Figure 2 shows selected data for a $\sim$7 week period around the time of April 18, which is indicated by a dashed line in the figure. Also, indicated by an arrow in Figure 2*a* is the time of the April 8 observing campaign, which occurred near the end of the rising phase of the outburst (Hynes et al. 2000).

The 2–12 keV X-ray data shown in Figure 2*a* are consistent with a mean intensity of $I_X = 2.89 \pm 0.41$ counts s^{-1} (rms), which corresponds to a relative intensity of 38 mcrab. Optical photometric data are shown in Figure 2*b*. For these data, we find mean magnitudes of $B = 13.02 \pm 0.04$ (rms) and $I = 12.68 \pm 0.05$ (rms). Figure 2*c* shows 15.2 GHz radio data with a mean flux density of $S_\nu = 8.68 \pm 0.87$ mJy (rms). Thus the rms variability of the source during this 7 week interval was 14% in the X-ray, 5% in the optical, and 10% in the radio. Moreover, much of this apparent variability is caused by measurement error. The typical measurement error for the ASM X-ray detectors was $\pm$10% (Fig. 2*a*), and for the Ryle Telescope it was $\pm$5% (Fig. 2*c*). Thus we conclude that for several weeks around April 18, XTE J1118+480 was stable in intensity to better than 10% on timescales of $\sim$1 day in the radio, optical, and X-ray bands.

Because of the long-term stability of the source, we have summed 16 consecutive *RXTE* spectra obtained between April 13.39 and May 15.38 in order to improve the counting statistics above 100 keV. We used the analysis techniques described in § 2. These 16 observations can all be fit individually by a power-law model with photon indices that range between 1.77 and 1.81. The summed spectrum has a total integration time of 45.9 ks in the PCA and 16.8 ks in the HEXTE (only cluster A was used). A power-law model fit the summed spectrum with $\Gamma = 1.779 \pm 0.003$ for a χ^2 of

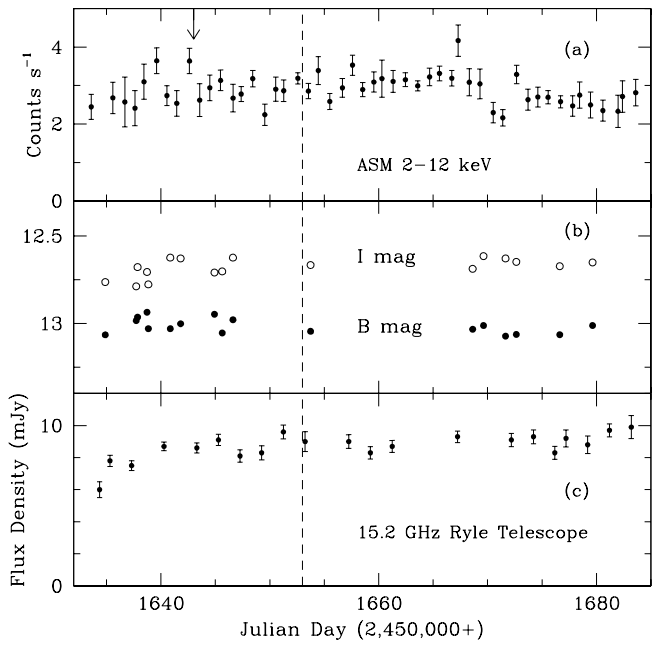

FIG. 2.—Seven-week record of the intensity of XTE J1118+480 measured at X-ray, optical, and radio frequencies. The dashed line corresponds to 2000 April 18.5 UT, the nominal time of the intensive observing campaign reported on herein. The arrow is drawn at 2000 April 8.5 UT, the nominal time of the observations conducted by Hynes et al. (2000). (*a*) 2–12 keV *RXTE* ASM light curve. The data shown are daily-average intensities, which were obtained from the MIT ASM web page. (*b*) *UBVRI* optical photometric data were obtained on 17 occasions using the 1.2 m telescope at the F. L. Whipple Observatory. Only the *B* and *I* light curves are shown here. (*c*) 15.2 GHz radio light curve obtained using the Ryle Telescope.

116 for 95 dof. The best-fit power law that includes a simple exponential cutoff at high energies, i.e., $N(E) \propto E^{-\Gamma} e^{-E/E_c}$, yielded a cutoff energy of 940 keV for a χ^2 of 103 for 94 dof. Arbitrarily fixing the cutoff energy at 300 keV produced an unacceptable fit with a χ^2 of 150 for 95 dof. Of course, these results do not rule against an abrupt, breaking cutoff at energies of $\sim$150 keV since these energies are near the limit of HEXTE's response. Compared to the simple power-law model, a somewhat poorer fit to the data was achieved using a Comptonization model ("compTT" in XSPEC; Arnaud & Dorman 2000; Titarchuk 1994) with an electron temperature of 207 keV and an optical depth of 1.0 for a χ^2 of 125 for 94 dof.

4. THE SPECTRAL ENERGY DISTRIBUTION

The most difficult problem in constructing the SED is in properly correcting the EUV fluxes for IS absorption. It is not possible to obtain a precise measurement of $N_{\rm H}$, the IS column depth. For example, 21 cm measurements imply $N_{\rm H} = 1.34 \times 10^{20}$ cm^{-2} (Dickey & Lockman 1990). On the other hand, the *COBE* maps of dust IR emission imply $N_{\rm H} = 0.67 \times 10^{20}$ cm^{-2} (Schlegel, Finkbeiner, & Davis 1998). However, neither of these values can be considered secure, since $N_{\rm H}$ can vary by a factor $\sim$2 on much smaller angular scales than those probed by the surveys just mentioned (Faison et al. 1998). A line-of-sight estimate of $N_{\rm H}$ using the Ca II lines implies a high value: $N_{\rm H} = 2.8 \times 10^{20}$ cm^{-2}; however, the uncertainty in log ($N_{\rm H}$) is at least 0.2 (Dubus et al. 2001). The source was too faint to make a 21 cm absorption measurement feasible.

There is an additional complication with the IS absorption in the EUV: A significant fraction of the absorption near 0.1 keV is attributable to neutral and ionized helium; however, there are no existing data on the absorbing columns for this line of sight. Rigorous inclusion of He absorption based on only the neutral hydrogen column would then require knowledge of both the line-of-sight hydrogen and helium ionization fractions, as well as the abundance of helium relative to hydrogen. Consequently, we estimate the IS absorption, parameterized by $N_{\rm H}$, by assuming the neutral and ionized He number densities relative to that of neutral hydrogen stated in § 2. Given all of these uncertainties, we, like Hynes et al. (2000), chose to estimate $N_{\rm H}$ by examining the SED itself.

In Figure 3 we show four realizations of the SED for four assumed values of $N_{\rm H}$. Here we have omitted the infrared and radio data. At energies above a few tenths of a keV, the spectrum can be described in terms of a power law with varying spectral index as follows. At the highest energies, the photon index is $\approx$1.78 (§§ 2 and 3). At energies below $\sim$2 keV, the spectrum becomes harder and the photon index approaches $\approx$1.5. It is possible that the systematic errors discussed in § 2 contribute to this hardening of the spectrum; however, it is unlikely that they can account for all of it.

The only appreciable gap in the SED is centered at log (ν) $\approx$ 16.0, where the ISM is opaque. We now focus on the question of how to connect the *HST* data with the *EUVE* data across this unobserved region. It is apparent from Figure 3 that the dereddened *EUVE* spectrum is very sensitive to the choice of $N_{\rm H}$ and is consequently very uncertain. Therefore, we first consider the high-quality *HST* spectrum, which depends weakly on the choice of reddening. We can be confident that the *HST* spectrum is made up of

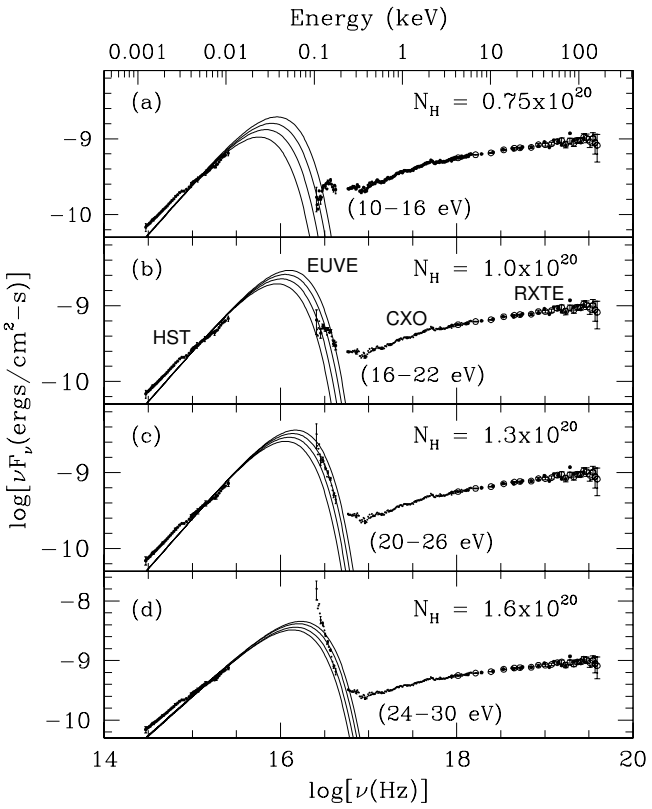

FIG. 3.—Four realizations of the SED for the indicated values of the column density. Inspection of panels (*a*)–(*d*) shows that the *HST* UV spectrum and the low-energy portion of the *Chandra* X-ray spectrum are only mildly sensitive to the choice of $N_{\rm H}$. However, the *EUVE* spectrum is extremely sensitive. Solid curves represent multicolor disk blackbody model spectra, which have been normalized to the *HST* flux at log (ν) = 15.1. Models are specified by the temperature at the inner edge of the accretion disk, $T_{\rm in}$. The four models in each panel are equally spaced by 2 eV, and the lowest and highest values of k$T_{\rm in}$ are indicated in the figure.

substantial thermal emission because the Balmer jump in absorption is apparent at log (ν) $\approx$ 14.9. In the following, we assume that the UV emission is caused chiefly by the accretion disk (see § 5).

We therefore consider the simple model spectrum of a steady accretion disk as implemented in XSPEC (Arnaud & Dorman 2000; Mitsuda et al. 1984; Makishima et al. 1986). We do not include a power-law component, which would increase the *EUVE* model fluxes somewhat. These multicolor disk blackbody spectra are meant to be illustrative; they are not fits to the data. Each disk spectrum shown in Figure 3 is specified by two parameters: (1) the temperature at the inner edge of the disk, $T_{\rm in}$, and (2) the normalization, which we arbitrarily take to be the dereddened *HST* flux at log (ν) = 15.1. We first consider the SED for $N_{\rm H} = 1.6 \times 10^{20}$ cm^{-2} (Fig. 3*d*). We find that no simple disk spectrum can match the steeply rising *EUVE* spectrum, and the mismatch is only worse for higher values of $N_{\rm H}$. We therefore do not consider values of $N_{\rm H} \gtrsim 1.6 \times 10^{20}$ cm^{-2} further.

We next examine $N_{\rm H} = 0.75 \times 10^{20}$ cm^{-2}, which is illustrated in Figure 3*a*. By considering the *EUVE* data as part of the nonthermal spectrum (see Hynes et al. 2000), it is possible to accommodate a thermal disk component with $kT_{\rm in} \lesssim 12$ eV. However, the comparison of the model to the data is somewhat unsatisfying for two reasons. First, Hynes et al. made the reasonable assumption that the EUV and

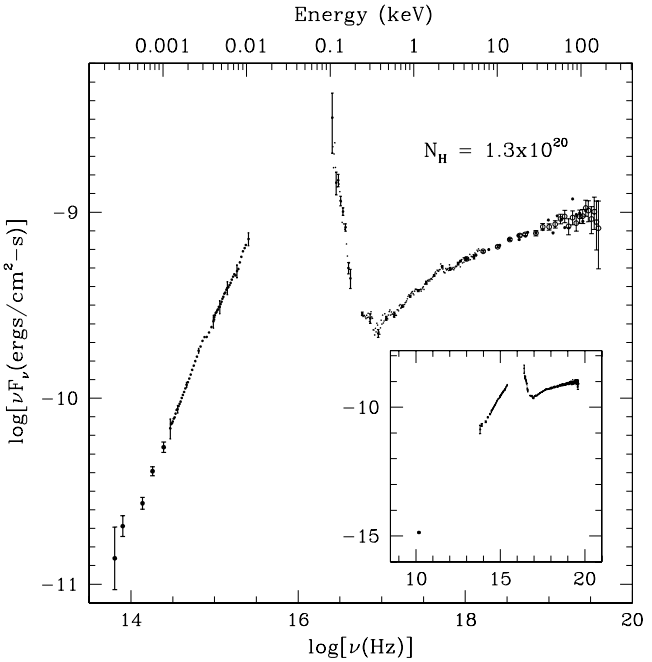

FIG. 4.—Enlargement of the SED corrected for the adopted column depth of $N_H = 1.3 \times 10^{20}$ cm^{-2}. This is the same SED shown in Fig. 3c, except that the infrared data are included here. The inset shows all of the same data plus the 15.2 GHz radio data for April 18. The following comments about the individual data sets apply also to Fig. 3: (1) UKIRT flux densities reported by Hynes et al. (2000) have been multiplied by 0.8 to force them to approximately match the *HST* spectrum; the discrepancy may be because of the short UKIRT exposures and the rapid optical variability of the source (Patterson 2000). (2) *HST* data were dereddened (Cardelli, Clayton, & Mathis 1989; Predehl & Schmitt 1995). No ad hoc corrections have been applied to these data; error bars are plotted on every eighth point. (3) *EUVE* data become quite uncertain near the lowest energy (0.10 keV); error bars are displayed on approximately every third data point. (4) *Chandra* LETG spectrum has very small statistical errors; error bars are drawn on every tenth data point. The spectrum shown here is truncated at 6 keV; otherwise, no ad hoc corrections have been made to this spectrum. (5) *RXTE* data begin at 3 keV and thus overlap substantially with the LETG spectrum. Small filled circles without error bars show the spectrum for April 18. The summed spectrum (§ 3) is plotted as open circles with error bars. The statistical significance of the last two data points in the summed spectrum are 3.8 σ at 154 keV and 2.8 σ at 162 keV. Since Crab observations indicate that *RXTE* systematically produces fluxes that are high by about 15%, and since some modest variability is expected, the fluxes for April 18 were multiplied by 0.84 to match the overlapping LETG fluxes; similarly, the summed-spectrum fluxes were multiplied by 0.91.

hard X-ray fluxes were approximately fitted by the same power law; however, the *Chandra* data complicate this picture by revealing a wider range of power-law slopes. Second, the structure in the *EUVE* spectrum is not easily explained, although it may possibly be attributable to the presence of a warm absorbing medium around the source (see Esin et al. 2001). In short, we consider $N_H = 0.75 \times 10^{20}$ cm^{-2} a viable choice; however, we do not favor it. Even lower values of N_H appear less likely since at long wavelengths the *EUVE* spectrum plunges downward (Hynes et al. 2000) and has the wrong inflection to join up with the model disk spectra.

We favor the two remaining spectra shown in Figures 3*b* and 3*c*. First consider the case $N_H = 1.3 \times 10^{20}$ cm^{-2} (Fig. 2*c*). This case provides the closest match between one of the model disk spectra ($kT_{in} = 24$ eV) and the *EUVE* spectrum. $N_H = 1.3 \times 10^{20}$ cm^{-2} probably corresponds to an upper limit on the value of N_H since there may be a significant nondisk component of UV emission at log (ν) = 15.1 (see § 5). In this case, the disk spectra in Figure 3*c* would need to be renormalized downward, thereby creating some disagreement between the data and the models: i.e., the *EUVE* data would then rise more steeply than the models (cf. Fig. 3*d*).

Finally, consider the spectrum for $N_H = 1.0 \times 10^{20}$ cm^{-2} (Fig. 3*b*). At short wavelengths, the *EUVE* spectrum conforms closely to the model for $kT_{in} = 22$ eV, whereas at longer wavelengths it straddles the models for $kT_{in} = 18$–22 eV. If the normalization of the disk models were to be corrected downward (as mentioned above), this model would provide a better description of the data. In short, we conclude that the most probable value of the column density lies in the range $N_H = 1.0$–1.3×10^{20} cm^{-2}. In the following, we adopt $N_H = 1.3 \times 10^{20}$ cm^{-2} and the version of the SED shown in Figure 3*c*. This spectrum, including the infrared and radio data, is reproduced in more detail in Figure 4; see the legend for further details about the individual data sets. The data shown in Figure 4 are available in digital form by request: for the *HST* data contact C. Haswell or R. Hynes; for the remaining data contact J. McClintock.

5. DISCUSSION

Most black hole X-ray novae in outburst reach the *high/soft* state (van der Klis 1994) and spend considerable time there; consequently, most X-ray novae are observed in this state. The high/soft state is dominated by a $\sim$1 keV blackbody-like spectral component, which is widely attributed to an accretion disk with its inner edge at or near $R_{in} = 3R_{Schw}$ ($R_{Schw} = 2GM/c^2$), the radius of the innermost stable orbit (Tanaka & Lewin 1995). A very simple and successful model for this thermal disk spectrum is the multicolor disk blackbody model (§ 3; Mitsuda et al. 1984; Makishima et al. 1986).

A few X-ray novae have been observed only in the *low/hard* state: e.g., V404 Cyg, GRO J0422+32, and GS1354−64 in 1997 (Brocksopp et al. 2001). A number of canonical X-ray novae (e.g., Nova Mus 1991 and GS2000+25) and Cyg X-1 have also been observed in the low/hard state (Tanaka & Lewin 1995). For the sources observed in this state, the nonstellar optical/UV spectrum has provided evidence for the presence of an outer accretion disk. However, for these sources it has not been possible to determine directly the properties of their inner disks, which emit in the EUV and soft X-ray bands, because of the high IS column depths: $N_H \gtrsim 10^{21}$ cm^{-2}. Observations of XTE J1118+480 with $N_H \approx 1.3 \times 10^{20}$ cm^{-2} provide the first detection of radiation from the inner accretion disk for an X-ray nova in the low/hard state.

A simple explanation for the low thermal temperature in XTE J1118+480 is that the inner edge of the accretion disk is quite far out compared to $R_{in} = 3R_{Schw}$. This is the expected state of affairs in some models of the low/hard state (e.g., Esin, McClintock, & Narayan 1997). Moreover, there is good indirect evidence based on Compton reflection models that such large, cool disks do exist in the low/hard state of several systems (e.g., see Gierlinski et al. 1997; Miller et al. 2001).

Based on our adopted value of N_H (§ 4) and a distance of 1.8 kpc (McClintock et al. 2001; Wagner et al. 2001), we can make a rough estimate of the inner disk radius for $kT_{in} = 24$ eV (Fig. 3*c*) as follows. For an intensity of 38 mcrab and a photon spectral index of 1.78 (§ 3), the 1–160 keV X-ray

luminosity is $L_X \approx 1.2 \times 10^{36}$ ergs s^{-1}. For an assumed value of the accretion efficiency, ϵ, the X-ray luminosity determines the mass accretion rate, $M = L_X/\epsilon c^2$, and hence the inner radius of a steady state disk: $R_{in} = (3GM_X\dot{M}/8\pi\sigma T_{in}^4)^{1/3}$ (e.g., Frank, King, & Raine 1992). For a canonical efficiency of 10%, we find $R_{in} = 60R_{Schw}$, and for an advection-dominated flow with an assumed efficiency of 0.1% we find $R_{in} = 285R_{Schw}$. A comparable value for R_{in} can be obtained by using the normalization constant determined for the multicolor disk blackbody model, which depends only on the solid angle subtended by the inner disk and the inclination of the disk (Arnaud & Dorman 2000). Assuming that the flux at log (ν) = 15.1 is caused solely by the disk (see below) and assuming a high inclination, $i = 80°$ (Wagner et al. 2001), we find $R_{in} = 34R_{Schw}$ for the model with $kT = 24$ eV shown in Figure 3*c*.

We note that the radio/IR data and the *HST* data below the Balmer jump can all be reasonably well fit by a single power law, $\nu F_\nu \propto \nu^{1.10}$, which steepens at longer radio wavelengths (Hynes et al. 2000). Thus, in the IR/radio band there is an additional component of emission above that expected for a multicolor disk blackbody spectrum (Hynes et al. 2000; Esin et al. 2001). This component may be associated with an outflow from the system (Esin et al. 2001; Fender 2001).

Could this IR/radio component affect our earlier conclusions on the temperature of the thermal accretion disk component? In § 4 we assumed that the UV flux is dominated by the spectrum of the accretion disk. This assumption is supported by the presence of a $\approx$0.09 mag Balmer jump in the spectrum. Unfortunately, the strength of the Balmer jump in absorption cannot be used to determine quantitatively the fraction of the total flux that is caused by the accretion disk. In a disk there are several conditions that can reduce or even eliminate the Balmer jump: e.g., high inclination and X-ray heating (la Dous 1989). Indeed, Balmer jumps are often absent or appear in emission in the spectra of dwarf novae (la Dous 1989; Williams 1983) and one was not detected in the spectrum of X-ray Nova Mus 1991 during outburst (Cheng et al. 1992). In short, we cannot rule out the hypothesis that the IR/radio component contributes to the UV spectrum of XTE 1118+480. However, the presence of a significant Balmer jump argues for appreciable disk emission. In this work, we assume that the disk flux is dominant in the UV band.

In conclusion, the global spectrum consists of three components: (1) $a \approx 24$ eV thermal component caused by the accretion disk with a large inner radius ($\gtrsim 35R_{Schw}$); (2) a quasi power-law component, which extends from $\sim$0.4 keV to at least 160 keV; and (3) a third component that dominates the spectrum at wavelengths greater than several microns. A model for the first two components and a discussion of the third one are presented in a companion paper by Esin et al. (2001).

We thank the *Chandra X-Ray Observatory* Director H. Tananbaum for granting Director's Discretionary Time, the entire *Chandra* team for their superb effort and enthusiasm, and NASA for providing support for J. E. M., M. R. G., and J. J. D. through grant DD0-1003X and contract NAS 8-39073. The *EUVE* observations were made possible by a generous grant of Director's Discretionary Time by *EUVE* Project Manager R. Malina, the efforts of *EUVE* Science Planner M. Eckert, the staff of the *EUVE* Science Operations Center at CEA, and the Flight Operations Team at Goddard Space Flight Center. This work includes observations with the NASA/ESA *Hubble Space Telescope*, obtained at the Space Telescope Science Institute, operated by the Association of Universities for Research in Astronomy, Inc., under NASA contract NAS 5-26555. We would like to thank the *HST* and *RXTE* support staff for ongoing efficient support. UKIRT is operated by the Joint Astronomy Centre on behalf of the UK Particle Physics and Astronomy Research Council. C. A. H., R. I. H., and S. C. acknowledge support from grant F/00-180/A from the Leverhulme Trust. J. E. M. acknowledges helpful discussions with A. Siemiginowska and N. Brickhouse. We thank an anonymous referee for several constructive comments.

REFERENCES

Arnaud, I., & Dorman, B. 2000, XSPEC (An X-Ray Spectral Fitting Package), version 11 (Greenbelt, MD: HEASARC, NASA/GSFC)
Brocksopp, C., Jonker, P. G., Fender, R. P., Groot, P. J., van der Klis, M., & Tingay, S. J. 2001, MNRAS, 323, 517
Cardelli, J. A., Clayton, G. C., & Mathis, J. S. 1989, ApJ, 345, 245
Cheng, F. H., Horne, K., Panagia, N., Shrader, C. R., Gilmozzi, R., Paresce, F., & Lund, N. 1992, ApJ, 397, 664
Dickey, J. M., & Lockman, F. J. 1990, ARA&A, 28, 215
Dubus, G., Kim, R. S. J., Menou, K., Szkody, P., & Bowen, D. V. 2001, ApJ, 553, 307
Esin, A. A., McClintock, J. E., Drake, J. J., Garcia, M. R., Haswell, C. A., Hynes, R. I., Marshall, H. L., & Muno, M. P. 2001, ApJ, 555, 483
Esin, A. A., McClintock, J. E., & Narayan, R. 1997, ApJ, 489, 865
Faison, M. D., Goss, W. M., Diamond, P. J., & Taylor, G. B. 1998, AJ, 116, 2916
Fender, R. P. 2001, MNRAS, 322, 31
Frank, J., King, A., & Raine, D. 1992, Accretion Power in Astrophysics (2d ed.; Cambridge: Cambridge Univ. Press)
Gierlinski, M., Zdziarski, A. A., Done, C., Johnson, W. N., Ebisawa, K., Ueda, Y., Haardt, F., & Phlips, B. F. 1997, MNRAS, 288, 958
Hynes, R. I., Mauche, C. W., Haswell, C. A., Shrader, C. R., Cui, W., & Chaty, S. 2000, ApJ, 539, L37
Jahoda, K. 2000, unpublished talk presented 2000 March 22 at the Rossi 2000 Symp. (Greenbelt, MD: GSFC/NASA)
la Dous, C. 1989, MNRAS, 238, 935
Makishima, K., Maejima, Y., Mitsuda, K., Bradt, H. V., Remillard, R. A., Tuohy, I. R., Hoshi, R., & Nakagawa, M. 1986, ApJ, 308, 635
Marshall, H. L., Carone, T. E., Shull, J. M., Malkan, M. A., & Elvis, M. 1996, ApJ, 457, 169
McClintock, J., Garcia, M., Caldwell, N., Falco, E. E., Garnavich, P. M., & Zhao, P. 2001, ApJ, 551, L147
Miller, J. M., Fox, D. W., Di Matteo, T., Wijnands, R., Belloni, T., Pooley, D., Kouveliotou, C., & Lewin, W. H. G. 2001, ApJ, 546, 1055
Mitsuda, K., et al. 1984, PASJ, 36, 741
Patterson, J. 2000, IAU Circ. 7412
Pooley, G. G., & Fender, R. P. 1997, MNRAS, 292, 925
Pooley, G. G., & Waldram, E. M. 2000, IAU Circ. 7390
Predehl, P., & Schmitt, J. H. M. M. 1995, A&A, 293, 889
Remillard, R., Morgan, E., Smith, D., & Smith, E. 2000, IAU Circ. 7389
Rhoades, C. E., & Ruffini, R. 1974, Phys. Rev. Lett., 32, 324
Rumph, T., Bowyer, S., & Vennes, S. 1994, AJ, 107, 2108
Schlegel, D. J., Finkbeiner, D. P., & Davis, M. 1998, ApJ, 500, 525
Tanaka, Y., & Lewin, W. H. G. 1995, in X-Ray Binaries, ed. W. Lewin, J. van Paradijs, & E. van den Heuvel (Cambridge: Cambridge Univ. Press), 126
Titarchuk, L. 1994, ApJ, 434, 570
Uemura, M., et al. 2000, PASJ, 52, L15
van der Klis, M. 1994, ApJS, 92, 511
Wagner, R. M., Foltz, C. B., Shahbaz, T., Casares, J., Charles, P. A., Starrfield, S. G., & Hewett, P. 2001, ApJ, in press
Williams, G. 1983, ApJS, 53, 523